Computational Investigation into Ligand Effects on Correlated Geared Dynamics in Dirhodium Supramolecular Gears – Insights Beyond the NMR Experimental Window

Ieva Liepuoniute, Jacob N. Sanders, Miguel A. Garcia-Garibay*, K. N. Houk*

Department of Chemistry and Biochemistry, University of California, Los Angeles, California 90095, United States
*mgg@chem.ucla.edu (MGG) and *houk@chem.ucla.edu (KNH)

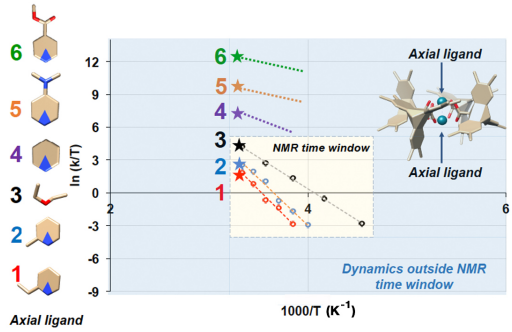

ABSTRACT: The rotational dynamics in dirhodium supramolecular gears, formed with four 9-triptycene carbocylates cyclically arranged around a dirhodium core with variable axial ligands as originally designed by Shionoya *et.al.,* provide an excellent opportunity to evaluate the potential of computational methods and expand our understanding of the factors determining geared dynamics. Rotational dynamic rates in these structures depend on the nature of the axial ligand as shown by simulations over time scales that are not accessible experimentally. Molecular dynamics simulations gave information on the gearing mechanism, and the activation barriers to gearing were calculated using density functional theory. Steric demands imposed by the axial ligand were quantified using buried volume analysis. We found that gearing takes place in all four dirhodium-gear complexes with different axial ligands, and that rotational barriers depend on their steric size.

INTRODUCTION

Molecular ensembles that display correlated motion comparable to that of macroscopic machinery could bring exciting new opportunities in materials science and nanotechnology.[1] The construction of molecular machines begins from careful consideration of molecular geometry, size, shape, nonbonding interactions, and electronic properties that dictate aggregation capabilities, dynamics, actuation possibilities, and mechanical functions.[1,2] Chemists can utilize these properties to combine molecules into systems that are capable of transducing energy or performing work from non-equilibrium states. Currently, research is focused on exploring different structural platforms and building blocks that allow for these functions.[3] A deeper understanding of the relation that exists between complex structural features at the molecular and supramolecular level and their coupled dynamics will make it possible to design machine-like functions involving correlated motions in the form of gearing.

Gearing is achieved when molecular rotors with cogs, or teeth, are tightly intermeshed.[4] Geared rotation implies that two or more adjacent rotors give up their individual degrees of freedom to enter a regime where the velocity and direction of rotation of any one element is dependent on the rotational characteristics of its closest neighbors.[3,5] To date, many molecular gear designs are based on the use triptycene as a three-toothed cog gear (Figure 1).[3-6]

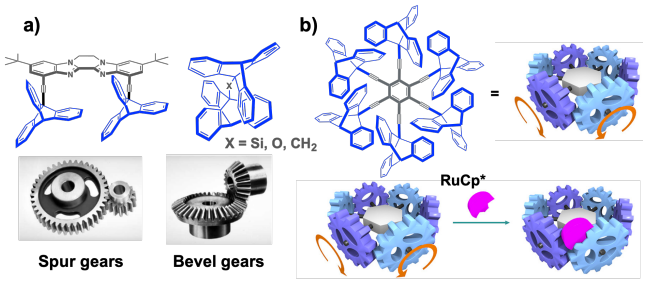

Figure 1. (a) Molecular spur and bevel gears, and their macroscopic analogues. b) Molecular structure of sextuple gear with six triptycene gears attached to the central benzene through an ethynyl linker and its schematic representation. Gearing rate is controlled by the addition of a bulky RuCp* complex to one of the gears of the molecule.

Triptycene units can adopt parallel or bent orientations resulting in spur or bevel gears, as illustrated by the two structures shown in Figure 1a. Triptycenes in spur gears lie in parallel alignment with the edge of a benzene ring of one triptycene fitting into the groove that exists between two benzene rings of an adjacent triptycene. In contrast, molecular bevel gears consist of two intermeshed three-bladed triptycene cogs linked by a single atom or *cis*-alkene derivative, and at an off-parallel angle.[5] Angle widening or narrowing imposes high strain on the system, preventing the gears from deviating from their intermeshed configuration. Notably, single-atom linkers exhibit a substantial angle widening due to steric hindrance exerted by triptycene groups.

While several strategies to construct molecular gears have been proposed, the efficient control of the rate and direction of synergistic motion between different molecular components remains challenging. Only a few successful examples of tunable gearing dynamics are known to date.[7,8] A complex multirotor gear consisting of six triptycene gears circularly arranged around a central benzene ring through ethynyl linkers reported by Shionoya *et.al.* showed switchable dynamics when a bulky ruthenium pentamethylcyclopentadienyl complex (RuCp*) was coordinatively attached as a chemical shim to one of the three phenylene rings of a triptycene gear (Figure 1b).[9] As a result, motion was severely restricted, but not completely stopped. We became interested in tunable gear design, where four triptycene carboxylates are coordinated to a dirhodium core in a paddle-wheel complex. The rhodium(II) centers coordinate to axial ligands installed on the vertical axis as shown in Figure 2.[10] The cyclic cog arrangement places adjacent triptycenes perpendicularly to each other, and imposes geometrical constraints that force a benzene ring of one triptycene moiety to fit intimately between two benzene rings of the adjacent unit (Figure 2).

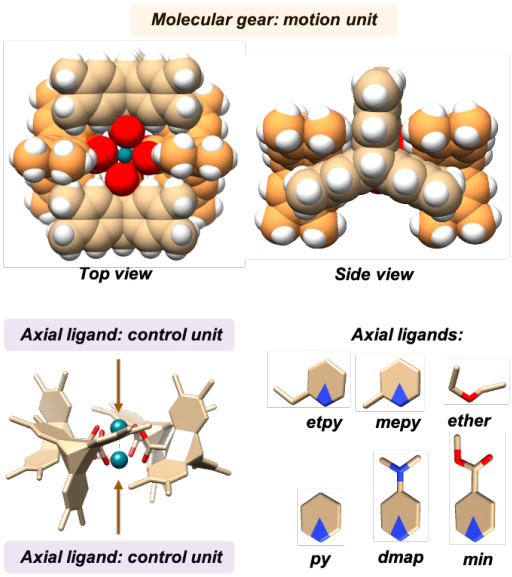

Figure 2. Space filling model of the paddle wheel four-gear dirhodium complex from top and side views. Axial ligands act as dynamic control units.

Overall, six different four-cog gear systems with different axial ligands were prepared and studied by Shionoya *et.al.*[10]: pyridine (*py*), 2-methylpyridine (*mepy*), 2-ethylpyridine (*etpy*), N,N-dimethyl-4-aminopyridine (*dmap*), methyl isonicotinate (*min*), and diethyl ether (*ether*) (Figure 3a). They carried out variable temperature (VT) ^{1}H NMR experiments in deuterated chloroform and showed that the rotational barrier for gearing changed upon installing different axial ligands. Such ligand-dependent dynamics were experimentally shown for *etpy*, *mepy*, and *ether* coordinated gears, but not in other rotor systems due to their motion being faster than the ^{1}H NMR time scales.[11] Indeed, given the small temperature range offered by typical NMR solvents, the small chemical shift difference between different conformers in ^{1}H NMR, and sample solubility limitations, the dynamic window observable experimentally provides information on gearing systems with rotational barriers higher than ca. 12 kcal/mol (Figure 3b). Molecular gearing events determined by lower barriers occur much faster and are time averaged by NMR, which calls for other approaches to study dynamics on these shorter time scales. Here we take advantage of computational techniques to study gearing dynamics on time scales ranging from nanoseconds to microseconds using molecular dynamics (MD) simulations and quantum mechanics (QM) calculations.[6d-f] Studies carried out with different axial ligands make it possible to analyze steric and electronic effects on the barriers for rotation. The results presented herein help understand how different axial ligands can modulate triptycene gear dynamics, and showcase an exciting tool for the design of molecular gears with dynamics in time scales of interest.

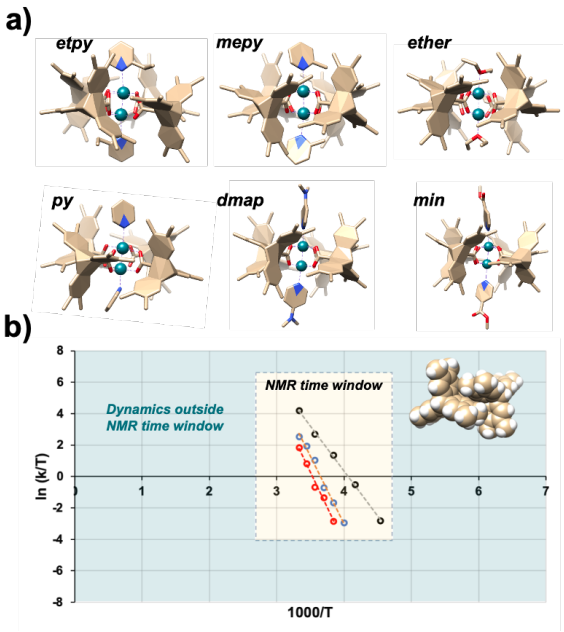

Figure 3. (a) Computational model of the four-gear dirhodium complex with different axial ligands with hydrogen atoms are omitted for clarity. The structures were obtained from X-ray diffraction experiments as reported by Shionoya and co-workers.[10] (b) The rotational rates and activation barriers could be determined by VT ^{1}H NMR only for *etpy*, *mepy*, and *ether* axial ligand systems. Gears with *py*, *dmap*, and *min* axial ligands could not be studied experimentally due to their dynamics being faster than the ^{1}H NMR time scales.

COMPUTATIONAL METHODS

Molecular dynamics (MD) simulations were performed using the GPU code (*pmemd.cuda*)[12] of the AMBER 16 package.[13]

Parameters for all gear systems were generated within the antechamber module using the general AMBER force field (*gaff*).[14] Parameters involving the Rh^{2+} ions were generated with the Metal Center Parameter Builder (*MCPB.py*)[15] using optimization and frequency calculations performed in Gaussian 09[16] at the B3LYP-D3(BJ)[17]/6-31G(d) level,[18] with the LANL2DZ[19] basis set and pseudopotential being used for the Rh^{2+} ions. Partial charges were set to fit the electrostatic potential generated at the HF/6-31G(d) level by the RESP model,[20] with the LANL2DZ basis set and effective core potential[21] being used for the Rh^{2+} ions. These partial charges were calculated according to the Merz–Singh–Kollman[22,23] scheme using Gaussian 09. Each molecular gear was immersed in a pre-equilibrated truncated octahedral box with a 15 Å buffer of chloroform molecules using the leap module. All subsequent calculations were done using the widely tested Stony Brook modification of the Amber14 force field (*ff14sb*).[24] Long-range electrostatic effects were modeled using the particle-mesh-Ewald method.[25] An 8 Å cutoff was applied to Lennard–Jones and electrostatic interactions. Initially, a geometry optimization was performed on each system to minimize the positions of solvent molecules while imposing positional restraints on the molecular gear using a harmonic potential with a force constant of 2 kcal·mol^{-1}·Å^{-2}. Next, each system was gently and continuously heated over 1 ns from 0 K to 300 K, 400 K, 450 K, and 500 K, respectively under constant-volume and periodic-boundary conditions. Harmonic restraints of 2 kcal·mol^{-1} were applied to each molecular gear and the Andersen equilibration scheme was used to control and equalize the temperature. The time step was kept at 1 fs during the heating stages, allowing potential inhomogeneities to self-adjust. Each system was then equilibrated for a total of 5 ns at constant pressure of 1 atm with a Berendson barostat with a 2 fs time step; harmonic restraints of 2 kcal·mol^{-1} were applied for the first 2 ns and harmonic restraints of 1 kcal·mol^{-1} were applied for the second 3 ns. Production trajectories without harmonic restraints were run for an additional 1 μs under the same simulation conditions.

All quantum mechanical (QM) calculations were performed using the Gaussian 09 software package.[16] Atomic coordinates of dirhodium gears were obtained from single crystal X-ray diffraction data as published by Shionoya and co-workers. Geometries were optimized in the gas phase using the B3LYP functional[17a,b] with Grimme's D3(BJ)[17c] dispersion correction, and with the 6-31G(d) basis set for all nonmetal atoms and the LANL2DZ effective core potential (ECP) for Rh. Single-point corrections were calculated using B3LYP-D3(BJ) functional with the 6-311+G(d,p)[26] basis set for all nonmetal atoms and the LANL2DZ the effective core potential for Rh. The transition state geometries were obtained by positioning the two intermeshed triptycene blades 30° off their optimized ground state geometries – half-way through the "gearing event." These transition states were then re-optimized using the conventional TS search method. Vibrational frequencies were computed to confirm that the optimized ground and transition state geometries correspond to minima and first order saddle points, respectively, on the potential energy surface. Quasi-harmonic thermodynamic Grimme's correction with a frequency cut-off of 100 cm^{-1} was calculated using the Goodvibes v3.01. software.[27] Solvent effects were included using the polarizable continuum model (PCM)[28] that accounts for electrostatic solute-solvent interactions.

Axial ligand steric effects were evaluated using the buried volume (%V_{bur}) parameter. Buried volume is defined as the percentage of volume in the first coordination sphere of the metal that is occupied by the ligand, and is a widely recognized model to describe steric properties of ligands.[29] The buried volume of different axial ligands (with hydrogen atoms included) was evaluated for each gear using the Samb*V*ca software.[30]

RESULTS AND DISCUSSION

MD simulations of the four-geared dirhodium complex with different axial ligands show that all complexes are gearing in an unhindered disrotatory manner, with adjacent triptycene gears turning in opposite directions (Supporting Information (SI) Movies 1-6). Conrotatory gear slippage where both gear units turn in the same directions is not observed. Rotational trajectories are analyzed by tracing the motion of each triptycene via dihedral angle changes which vary from –180° to 180º. The dihedral angle for each triptycene is defined as the angle between the plane of the carboxylates that coordinate to the dirhodium core and the plane of one of the triptycene blades (O-C_1-C_2-C_3) (Figure 4a). Triptycene has an overall D_{3h} symmetry and contains a three-fold axis of rotation with the blades separated by 120° degrees (Figure 4b). When two or more rotating triptycene moieties are positioned in such a way that their gearing profiles overlap, a gearing event can be defined as a 120° disrotatory flip between two adjacent triptycenes, where each triptycene blade is turning by 60° in the opposite direction.

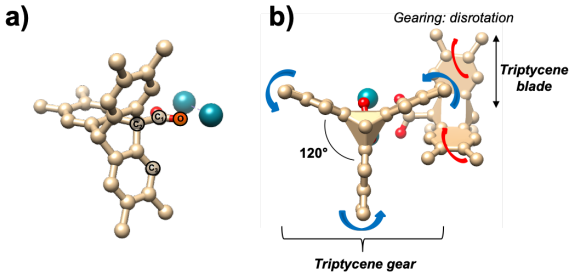

Figure 4. (a) Dihedral angle O-C_1-C_2-C_3 (atoms circled in black) is used to define triptycene rotation around the dirhodium core. (b) For a meshed triptycene system undergoing correlated rotation, gearing is observed when dihedral angles associated with different triptycene molecules are turning in opposite directions (disrotatory trajectory).

The initial MD trajectories performed at 300 K for 1 μs showed no gearing events for any of the systems, consistent with experimental observations.[10] Employing the Eyring kinetic theory and considering that experimental gearing enthalpies of activation evaluated at 260 K for *etpy*, *mepy*, and *ether* ligand-based gears were 18.0, 14.5, and 11.4 kcal·mol^{-1} respectively, we hypothesized that gearing dynamics could be observed at the microsecond timescale, but at much higher temperatures ranging from 400-500 K. Considering that the rotational barriers for gears with *dmap*, *min*, and *py* ligands are predicted to be lower than 12 kcal·mol^{-1}, we performed the next set of MD simulations at 400 and 450 K. These temperatures were sufficient to induce gearing events in *dmap*, *min*, and *py*, but not in *etpy*, *mepy*, and *ether* ligand-based gears. Given the highly correlated dynamics between the four

.

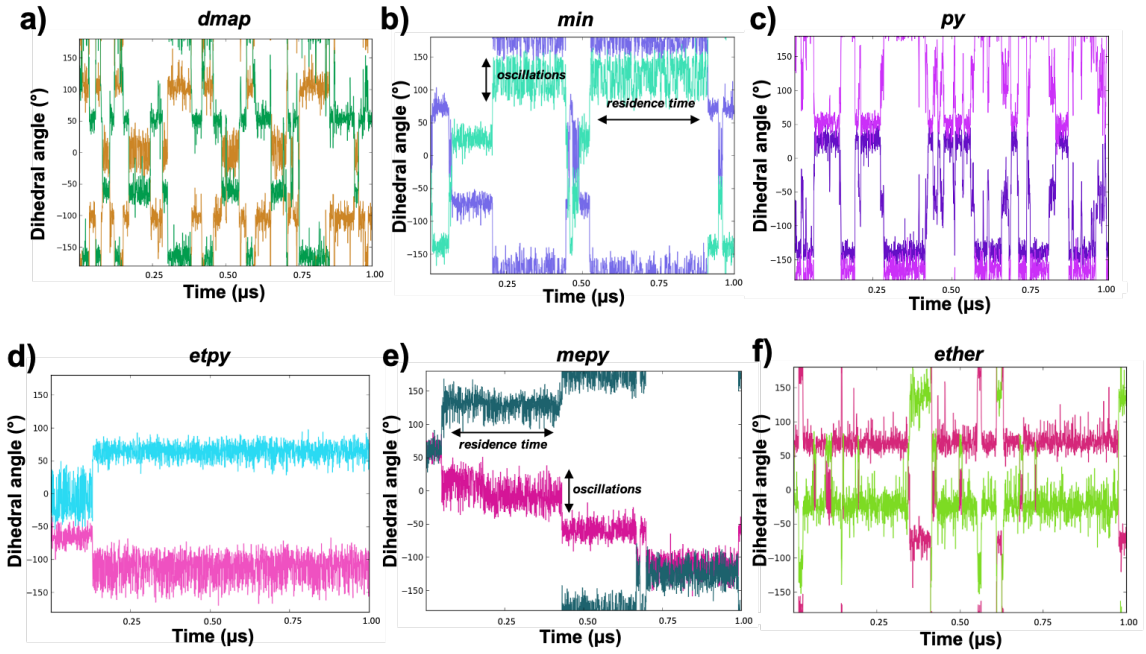

Figure 5. Dynamic simulations of triptycene gearing carried out for 1μs at 450 K (a-c) and 500 K (d-f) in four-geared dirhodium complexes with different axial ligands: (a) *dmap*, (b) *min*, (c) *py*, (d) *etpy*, (e) *mepy*, and (f) *ether*. Different colors in each plot represent dihedral angle values for the two intermeshed triptycene gears. A gearing event is observed when a dihedral angle for each gear is changing by 60° in opposite directions.

triptycene gears positioned in a tightly meshed configuration, we set out to track dihedral angle changes of two adjacent triptycenes while other two followed correspondingly. Plotting the dihedral angle evolution shows that as one triptycene gear is changing its dihedral angle in one direction by 60°, the other simultaneously responds in the opposite direction (Figure 5), as required for geared rotation. The dihedral angle evolution at 450 K in the *dmap*, *min*, and *py* axial ligand complexes undergoes torsional angle oscillations with an amplitude of ca. ±40° for *min* and ca. ±20° for *dmap* and *py* between gearing events. As shown in Figure 5 (a-c), rotations occur at irregular intervals in discrete ±60° jumps with a long residence time for *min* and much shorter times for *dmap* and *py* axial ligand systems. The dynamics of four-geared dirhodium complex with *etpy*, *mepy*, and *ether* ligands show dihedral angle oscillations of ca. ± 20° with no rotations occurring within the simulated 1 μs time window at 400 or 450 K. Repeating MD simulations at 500 K of *etpy*, *mepy*, and *ether* complexes showed gearing with discrete jumps of ±60° (Figure 5 d-f). The simulated dynamics are characterized by a distribution of residence times ranging from a few hundred picoseconds (*ether*, Figure 5f) to a few nanoseconds (*mepy*, Figure 5e). Only one gearing event is observed in *etpy* axial ligand gear (Figure 5d) due to its high rotational barrier in relation to the other gear systems. MD trajectories obtained for axial ligands at all temperatures in the microsecond time window reveal oscillations between disordered positions. Ligand bending from the Rh-Rh bond axis vary from ±3° for *py* to ~±10-15° for *etpy*, *dmap*, and *min* ligands (Figure 6). This result is in line with the experimental X-ray diffraction results where axial ligand bending motion took on a range of values, with bulkier axial ligands showing larger angle displacements. A careful analysis of MD results indicates that ligand dynamics and triptycene rotation fall under two different dynamic regimes, with ligand dynamics being three orders of magnitude faster than triptycene gearing. No coupled correlated motion is observed between axial ligands and triptycene gears due to the mismatch in their dynamic windows.

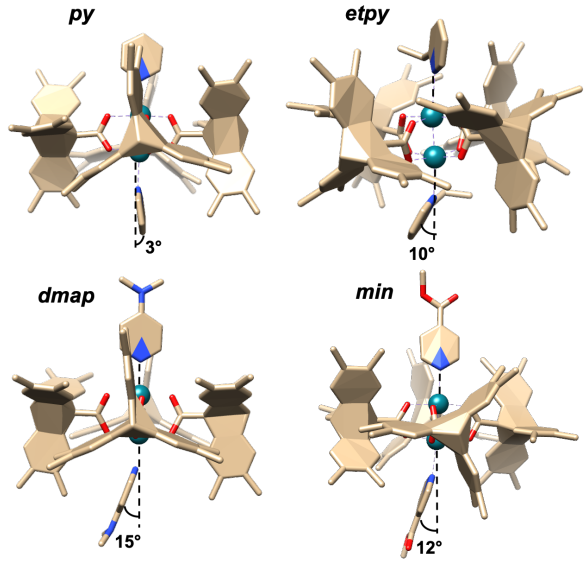

Figure 6. Axial ligand displacement with respect to the Rh-Rh bond axis took on a wide range of values: ±3° for *py* and ~±10-15° for *etpy*, *dmap*, and *min* ligands. Axial ligand motion was faster than triptycene gearing.

Axial ligand dynamics for *ether* are distinct from others. A close inspection of the van der Waals contacts between the diethyl ether axial ligand and triptycene blades shows that the ethyl moieties are always found in the notch between two benzene rings in triptycene molecules facing opposite each other. Notably, unlike any other axial ligand system studied, diethyl ether undergoes conformational flipping in addition to inertial

rotation around the Rh-Rh bond axis (Figure 7). Conformational motion occurs on a nanosecond time scale implying a low barrier (~2 kcal·mol^{-1}). Such fast ligand dynamics result in steric clashes between the diethyl moiety and triptycene blade causing more frequent triptycene dihedral angle oscillations with displacements of ca. ± 30° (Figure 4f).

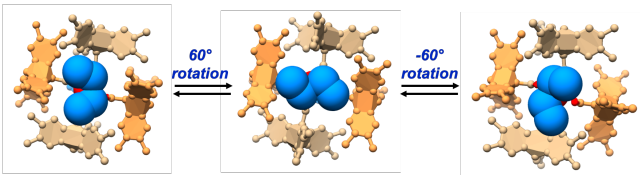

Figure 7. Triptycene gearing with diethyl ether as an axial ligand. A ball and stick model with filled planes was used to represent triptycene gears and a space-filling model was used for the axial ligand. Dynamic simulations were run for 1μs at 500 K. Diethyl ether shows rapid rotational motion around the Rh-Rh bond axis that is accompanied by conformational flipping. Axial ligand dynamics are accompanied by a 60° back-and-forth rotation of triptycene molecules.

Next, we employed QM calculations to evaluate the rotational barriers by comparing the energies of the ground and transition state structures for different four-geared dirhodium complexes (Figure 8). Enthalpies of activation, calculated in the gas phase at 260 K, match well with the experimental results obtained at the same temperature. We found that the gearing transition state is 12.5 kcal·mol^{-1} above the ground state for *etpy*, 12.1 kcal·mol^{-1} for *mepy*, and 7.1 kcal·mol^{-1} for *ether*. Rotational barriers for *py*, *dmap*, and *min* were found to be 5.5 kcal·mol^{-1}, 5.1 kcal·mol^{-1}, and 4.6 kcal·mol^{-1}, respectively. The barriers obtained for the solvated model are within 0.2 kcal·mol^{-1} of the barriers calculated in gas phase. Notably, the implicit solvent model does not correct the enthalpies to better match the experimental results. Ligands with electron-donating or election-withdrawing groups at a *para*-position on the pyridine axial ligand are ineffective at changing the rotational barrier. Gears with electron-donating group (*dmap*) and electron-withdrawing group (*min*) axial ligands have barriers that are only 0.1-0.2 kcal·mol^{-1} apart. In contrast, ligands bearing bulky substituents at the *ortho*-position showed ~10 kcal·mol^{-1} rotational barrier increases compared to the unsubstituted pyridine. We propose that such large changes in rotational barriers are due to steric clashes found between the axial ligand and triptycene blades, resulting in a more strained gear system. The rotational barrier increases as the steric size of the *ortho*-substituent increases.

Given that our employed DFT solvent model only represents solvent as a homogeneous polarizable medium instead of "explicit" solvent molecules, we expect that some of the solvent-triptycene steric interactions that could play a role in tuning the rotational barrier are not accounted for in our QM model. Even though triptycene gears are tightly intermeshed and solvent molecules cannot readily access the sites between triptycene blades, multiple access points are available around the axial ligand. Specifically, solvent molecules could be trapped in between the axial ligand and triptycene blades resulting in steric hindrance and leading to rotational barriers that are closer to experimentally determined values.

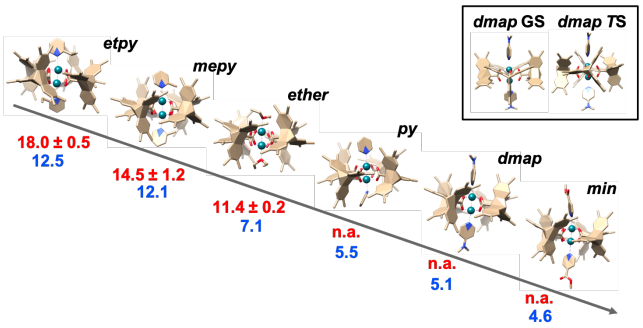

Figure 8. Enthalpies of activation for triptycene gears with different axial ligands. Experimental barriers are indicated in red and calculated barriers (at 260 K) are indicated in blue. The barriers were calculated by comparing enthalpies in ground and transition states (top right corner) for all axial ligand systems. All indicated energies are in kcal·mol^{-1}.

Finally, we sought to quantify the steric properties of these ligands using numerical parameters and search for statistical correlations with the observed rotational barriers. We employed the "buried volume" (%V_{bur}) analysis to quantify steric demands and the average bulkiness of axial ligands around the dirhodium core. Buried volume emphasizes steric hindrance close to the metal by measuring the volume occupied by the ligand in the first coordination sphere of the metal (Figure 9a). The plot of rotational enthalpies versus %V_{bur} (Figure 9b) illustrates that a ligand possessing a high buried volume corresponds to a large rotational barrier for triptycene gearing.

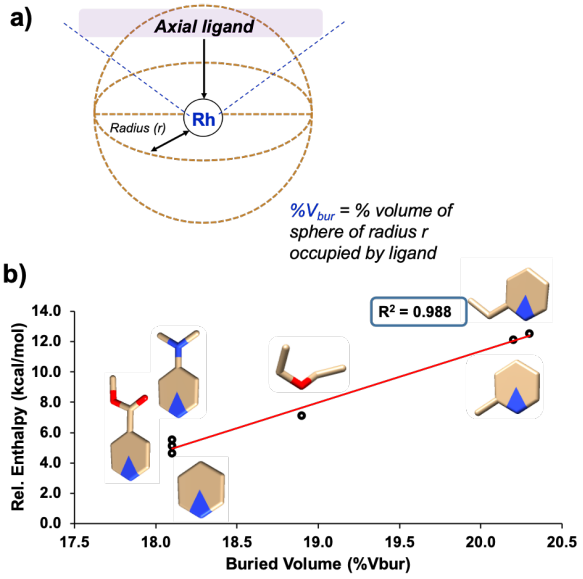

Figure 9. (a) Definition of buried volume (%V_{bur}) that evaluates steric encumbrance of axial ligands. (b) Linear relation between steric size of the axial ligand and rotational enthalpies of activation as calculated using DFT in gas phase at 260 K.

Overall, the calculated %V_{bur} for different axial ligands correlates well with the observed dynamic behavior of triptycene gears, with steric repulsions in the region of the axial ligand and triptycene blades playing a key role in tuning the rotational barrier. In contrast, substituents in the *para* position have no effect on the %V_{bur} values. Buried volume parameters were found to be identical for *py*, *dmap*, and *min* ligands, suggesting

that steric interactions between the triptycene molecules and the axial ligands are the same in all three systems. This observation matches the QM calculations that indicate minimal differences in enthalpy of activation among *py*, *dmap*, and *min*.

CONCLUSIONS

The origin of gearing dynamics in dirhodium-centered supramolecular triptycene gears with different axial ligands has been established by computational methods. Molecular dynamics simulations and density functional theory computations were used to explore gearing dynamics in time domains that are experimentally inaccessible. Molecular dynamics simulations provided good qualitative agreement with the expected gearing kinetics, and confirmed gearing in all four-geared dirhodium complexes with different axial ligands. DFT calculations for geared rotation reproduced the experimental trend in rotational barrier for *etpy*, *mepy*, and *ether* axial ligand systems, and predicted enthalpies of activation of 5.5, 5.1, and 4.6 kcal·mol^{-1} for *py*, *dmap*, and *min* ligand-based gears, respectively. Buried volume analysis served as a useful guide to understand the origins of axial ligand effects on gearing. Rotational dynamics were affected by the nature of the axial ligand via a steric interaction between axial ligand and the triptycene molecules. There is a direct correlation between the buried volume of the axial ligand and the rotational energy barrier, with the barrier increasing with the steric size of the *ortho*-substituent. The qualitative and quantitative consistency among the experimental and computational results helps establish that rotation of the dirhodium-based triptycene gears with different axial ligands occurs in the millisecond regime for *etpy*, *mepy*, and *ether*, and in the microsecond regime for *min*, *py*, and *dmap* axial ligand-based gears, and constitutes an example where the nature of the axial ligand can change the gearing rate by three orders of magnitude.

ASSOCIATED CONTENT

Supporting Information

Buried volume analysis, energies and vibrational frequencies, and optimized geometries of all species (PDF). Movies of molecular dynamics simulations of molecular gears **1**-**6** (MP4). The Supporting Information is available free of charge on the ACS Publications website.

AUTHOR INFORMATION

Corresponding Authors

* Miguel A. Garcia-Garibay - mgg@chem.ucla.edu
* K. N. Houk - houk@chem.ucla.edu

Funding Sources

This work was supported by National Science Foundation grants (DMR-1700471 to MGG and CHE-1764320 to KNH). Computations were performed on the Hoffman2 cluster at UCLA and the Extreme Science and Engineering Discovery Environment (XSEDE), which is supported by the NSF (OCI-1053575)

Notes

The authors declare no competing financial interest.

ACKNOWLEDGMENT

We thank the National Science Foundation for support of this work through grant DMR-1700471 and CHE-1764320

REFERENCES

(1) Recent reviews for artificial molecular machines, see: (a) Erbas-Cakmak, S.; Leigh, D. A.; McTernan, C. T.; Nussbaumer, A. L. Artificial Molecular Machines. *Chem. Rev.* **2015**, *11*, 10081–10206. (b) Vogelsberg, C. S.; Garcia-Garibay, M. A. Crystalline molecular machines: function, phase order, dimensionality, and composition. *Chem. Soc. Rev.* **2012**, *4*, 1892–1910. (c) Garcia-Garibay, M. A. Crystalline molecular machines: Encoding supramolecular dynamics into molecular structure. *Proc. Nat. Acad. Sci. U. S. A.* **2005**, *102*, 10771–10776. (d) Balzani, V.; Credi, A.; Raymo, F. M.; Stoddart, J. F. Artificial Molecular Machines. *Angew. Chem. Int. Ed.* **2000**, *39*, 3348–3391. (e) Kay, E. R.; Leigh, D. A.; Zerbetto, F. Synthetic Molecular Motors and Mechanical Machines. *Angew. Chem. Int. Ed*. **2007**, *46*, 72–191. (f) Browne, W. R.; Feringa, B. L. Making molecular machines work. *Nature Nanotech.* **2006**, *1*, 25–35.

(2) Karim, A. R.; Linden, A.; Baldridge, K. K.; Siegel, J. S. Symmetry and polar-π effects on the dynamics of enshrouded arylalkyne molecular rotors. *Chem. Sci.* **2010**, *1*, 102–110.

(3) (a) Kottas, G. S.; Clarke, L. I.; Horinek, D.; Michl, J. Artificial Molecular Rotors. *Chem. Rev.* **2005**, *105*, 1281–1376. (b) Khuong, T.-A. V.; Nuñez, J. E.; Godinez, C. E.; Garcia-Garibay, M. A., Crystalline Molecular Machines: A Quest Towards Solid State Dynamics and Function. *Acc. Chem. Res.* **2006**, *39*, 413-422.

(4) Frantz, D. K.; Baldridge, K. K.; Siegel, J. S. Applications of Structural Principles to the Design of Triptycene-Based Molecular Gears with Parallel Axes. *Chimia*, **2009**, *63*, 201-204.

(5) (a) Iwamura, H.; Mislow, K. Stereochemical consequences of dynamic gearing. *Acc. Chem. Res.* **1988**, *21*, 175–182. (b) Kawada, Y.; Iwamura, H. Phase Isomerism in Gear-Shaped Molecules. *Tetrahedron Lett.* **1981**, *22*, 1533–1536. (c) Kawada, Y.; Iwamura, H. Correlated rotation in bis(9- triptycyl)methanes and bis(9-triptycyl) ethers. Separation and interconversion of the phase isomers of labeled bevel gears. *J. Am. Chem. Soc.* **1983**, *105*, 1449–1459. (d) Kawada, Y.; Sakai, H.; Oguri, M.; Koga, G. Preparation of and dynamic gearing in cis-1,2-bis(9-triptycele)ethylene. *Tetrahedron Letters* **1994**, *35*, 139-142.

(6) Key articles on bevel and spur gears: (a) Kawada, Y.; Iwamura, H. Bis(4-chloro-1-triptycyl) ether. Separation of a pair of phase isomers of labeled bevel gears. *J. Am. Chem. Soc.* **1981**, *103*, 958–960. (b) Toyota, S.; Shimizu, T.; Iwanaga, T.; Wakamatsu, K. Structures and Conformational Analysis of 1,8-Bis(9-Triptycylethynyl) Anthracene and Its Derivatives as Prototypes of Molecular Spur Gears. *Chem. Lett.* **2011**, *40*, 312–314. (c) Kawada, Y.; Yamazaki, H.; Koga, G.; Murata, S.; Iwamura, H. Bis(9- triptycyl)amines, a missing link between the corresponding methanes and ethers. An unconventional synthesis and influence of nitrogen configurational inversion on the coupled disrotatory trajectory. *J. Org. Chem.* **1986**, *51*, 1472–1477. (d) Frantz, D. K.; Linden, A.; Baldridge, K. K.; Siegel, J. S. Molecular Spur Gears Comprising Triptycene Rotators and Bibenzimidazole-Based Stators. *J. Am. Chem. Soc.* **2012**, *134*, 1528–1535. (e) Kaleta, J.; Michl, J.; Mézière, C.; Simonov, S.; Zorina, L.; Wzietek, P.; Rodríguez-Fortea, A.; Canadell, E.; Batail, P. Gearing Motion in cogwheel pairs of molecular rotors: weak-coupling limit. *CrystEngComm* **2015**, *17*, 7829–7834. (f) Lemouchi, C.; Iliopoulos, K.; Zorina, L.; Simonov, S.; Wzietek, P.; Cauchy, T.; Rodríguez-Fortea, A.; Canadell, E.; Kaleta, J.; Michl, J.; Gindre, D.; Chrysos, M.; Batail, P. Crystalline Arrays of Pairs of Molecular Rotors: Correlated Motion, Rotational Barriers, and Space-Inversion Symmetry Breaking Due to Conformational Mutations. *J. Am. Chem. Soc.* **2013**, *135*, 9366–9376.

(7) Huang, F.; Wang, G.; Ma, L.; Wang, Y.; Chen, X.; Che, Y.; Jiang, H. Molecular Spur Gears Based on a Switchable Quinquepyridine Foldamer Acting as a Stator. *J. Org. Chem.* **2017**, *82*, 12106–12111.

(8) Ube, H.; Yasuda, Y.; Sato, H.; Shionoya, M. Metal-centred azaphosphatriptycene gear with a photo- and thermally driven mechanical switching function based on coordination isomerism. *Nat. Commun.* **2017**, *8*, 14296.

(9) Ube, H.; Yamada, R.; Ishida, J.; Sato, H.; Shiro, M.; Shionoya, M. A Circularly Arranged Sextuple Triptycene Gear Molecule. *J. Am. Chem. Soc.* **2017**, *139*, 16470-16473.

(10) Sanada, K.; Ube, H.; Shionoya, M. Rotational Control of a Dirhodium-Centered Supramolecular Four-Gear System by Ligand Exchange. *J. Am. Chem. Soc.* **2016**, *138*, 2945–2948.
(11) Hesse, M.; Maier, H.; Zeeh, B. *Spectroscopic Methods in Organic Chemistry*; Thieme Publishing Group: Stuttgart, 2007.
(12) Salomon-Ferrer, R.; Götz, A. W.; Poole, D.; Le Grand, S.; Walker, R. C. Routine Microsecond Molecular Dynamics Simulations with AMBER on GPUs. 2. Explicit Solvent Particle Mesh Ewald. *J. Chem. Theory Comput.* **2013**, *9*, 3878–3888.
(13) Case, D. A.; Cerutti, D. S.; Cheatham, III, T. E.; Darden, T. A.; Duke, R. E.; Giese, T. J.; Gohlke, H.; Goetz, A. W.; Greene, D.; Homeyer, N.; Izadi, S.; Kovalenko, A.; Lee, T. S.; LeGrand, S.; Li, P.; Lin, C.; Liu, J.; Luchko, T.; Luo, R.; Mermelstein, D.; Merz, K. M.; Monard, G.; Nguyen, H.; Omelyan, I.; Onufriev, A.; Pan, F.; Qi, R.; Roe, D. R.; Roitberg, A.; Sagui, C.; Simmerling, C. L.; Botello-Smith, W. M.; Swails, J.; Walker, R. C.; Wang, J.; Wolf, R. M.; Wu, X.; Xiao, L.; York, D. M.; Kollman, P. A. AMBER 2017, University of California, San Francisco.
(14) Wang, J. M.; Wolf, R. M.; Caldwell, J. W.; Kollman, P. A.; Case, D. A. Development and Testing of a General Amber Force Field. *J. Comput. Chem.* **2004**, *25*, 1157–1174.
(15) Li, P.; Merz, K. M. MCPB.py: A Python Based Metal Center Parameter Builder. *J. Chem. Inf. Model.* **2016**, *56*, 599–604.
(16) Gaussian 09, Revision D.01, Frisch, M. J.; Trucks, G. W.; Schlegel, H. B.; Scuseria, G. E.; Robb, M. A.; Cheeseman, J. R.; Scalmani, G.; Barone, V.; Mennucci, B.; Petersson, G. A.; Nakatsuji, H.; Caricato, M.; Li, X.; Hratchian, H. P.; Izmaylov, A. F.; Bloino, J.; Zheng, G.; Sonnenberg, J. L.; Hada, M.; Ehara, M.; Toyota, K.; Fukuda, R.; Hasegawa, J.; Ishida, M.; Nakajima, T.; Honda, Y.; Kitao, O.; Nakai, H.; Vreven, T.; Montgomery, Jr., J. A.; Peralta, J. E.; Ogliaro, F.; Bearpark, M.; Heyd, J. J.; Brothers, E.; Kudin, K. N.; Staroverov, V. N.; Keith, T.; Kobayashi, R.; Normand, J.; Raghavachari, K.; Rendell, A.; Burant, J. C.; Iyengar, S. S.; Tomasi, J.; Cossi, M.; Rega, N.; Millam, J. M.; Klene, M.; Knox, J. E.; Cross, J. B.; Bakken, V.; Adamo, C.; Jaramillo, J.; Gomperts, R.; Stratmann, R. E.; Yazyev, O.; Austin, A. J.; Cammi, R.; Pomelli, C.; Ochterski, J. W.; Martin, R. L.; Morokuma, K.; Zakrzewski, V. G.; Voth, G. A.; Salvador, P.; Dannenberg, J. J.; Dapprich, S.; Daniels, A. D.; Farkas, O.; Foresman, J. B.; Ortiz, J. V.; Cioslowski, J.; Fox, D. J. Gaussian, Inc., Wallingford CT, 2013.
(17) (a) Becke, A. D. *J. Chem. Phys.* **1993**, *98*, 5648. (b) Lee, C.; Yang, W.; Parr, R. G. Results obtained with the correlations energy density functionals. *Phys. Rev. B: Condens. Matter Mater. Phys.* **1988**, *37*, 785. (c) Grimme, S.; Antony, J.; Ehrlich, S.; Krieg, H. A consistent and accurate *ab initio* parametrization of density functional dispersion correction (DFT-D) for the 94 elements H-Pu. *J. Chem. Phys.* **2010**, *132*, 154104.
(18) Hehre, W. J.; Ditchfield, R.; Pople, J. A. Self-Consistent Molecular Orbital Methods. XII. Further Extensions of Gaussian-Type Basis Sets for Use in Molecular Orbital Studies of Organic Molecules. *J. Chem. Phys.* **1972**, *56*, 2257−2261.
(19) (a) Dolg, M.; Wedig, U.; Stoll, H.; Preuss, H. Energy-adjusted ab initio pseudopotentials for the first row transition elements. *J. Chem. Phys.* **1987**, *86*, 866−872. (b) Andrae, D.; Haußermann, U.; Dolg, M.; Stoll, H.; Preu, H. *Ab initio* energy-adjusted pseudopotentials for the noble gases Ne through Xe: Calculation of atomic dipole and quadrupole polarizabilities. *Theor. Chem. Acc.* **1990**, *77*, 123−141.
(20) Bayly, C. I.; Cieplak, P.; Cornell, W.; Kollman, P. a. A Well-Behaved Electrostatic Potential Based Method Using Charge Restraints for Deriving Atomic Charges: The RESP Model. *J. Phys. Chem.* **1993**, *97*, 10269–10280.
(21) Hay, P. J.; Wadt, W. R. *Ab Initio* Effective Core Potentials for Molecular Calculations. Potentials for the Transition Metal Atoms Sc to Hg. *J. Chem. Phys.* **1985**, *82*, 270–283.
(22) Besler, B. H.; Merz, K. M.; Kollman, P. A. Atomic Charges Derived from Semiempirical Methods. *J. Comput. Chem.* **1990**, *11*, 431–439.
(23) Singh, U. C.; Kollman, P. A. An Approach to Computing Electrostatic Charges for Molecules. *J. Comput. Chem.* **1984**, *5*, 129–145.
(24) Maier, J. A.; Martinez, C.; Kasavajhala, K.; Wickstrom, L.; Hauser, K. E.; Simmerling, C. ff14SB: Improving the Accuracy of Protein Side Chain and Backbone Parameters from ff99SB. *J. Chem. Theory Comput.* **2015**, *11*, 3696–3713.
(25) Darden, T.; York, D.; Pedersen, L. Particle Mesh Ewald: An N·log(N) Method for Ewald Sums in Large Systems. *J. Chem. Phys.* **1993**, *98*, 10089–10092.
(26) T. Clark, J. Chandrasekhar, G. W. Spitznagel, and P. v. R. Schleyer, Efficient diffuse function-augmented basis-sets for anion calculations. 3. The 3-21+G basis set for 1st-row elements, Li-F, *J. Comp. Chem.* **1983**, *4*, 294–301.
(27) This approach produces Gibbs energies which correlate more closely with experiment than alternative quasi-harmonic corrections: Luccarell, J.; Jackson, K. E.; Hamilton, A. D.; Paton, R. S. in preparation.
(28) Tomasi, J.; Mennucci, B.; Cammi, R. Quantum Mechanical Continuum Solvation Models. *Chem. Rev.* **2005**, *105*, 2999–3094.
(29) (a) Hillier, A. C.; Sommer, W. J.; Yong, B. S.; Petersen, J. L.; Cavallo, L.; Nolan, S. P. A Combined Experimental and Theoretical Study Examining the Binding of N-Heterocyclic Carbenes (NHC) to the Cp*RuCl (Cp* = η^5-C_5Me_5) Moiety: Insight into Stereoelectronic Differences between Unsaturated and Saturated NHC Ligands. *Organometallics* **2003**, *22*, 4322–4326. (b) Cavallo, L.; Correa, A.; Costabile, C.; Jacobsen, H. J. Steric and electronic effects in the bonding of N-heterocyclic ligands to transition metals. *Organomet. Chem.* **2005**, *690*, 5407–5413. (c) Clavier, H.; Nolan, S. P. Percent buried volume for phosphine and N-heterocyclic carbene ligands: steric properties in organometallic chemistry. *Chem. Commun.* **2010**, *46*, 841–861.
(30) Falivene, L.; Credendino, R.; Poater, A.; Petta, A.; Serra, L.; Oliva, R.; Scarano, V.; Cavallo, L. SambVca 2. A Web Tool for Analyzing Catalytic Pockets with Topographic Steric Maps. *Organometallics* **2016**, *35*, 2286–2293.